ELSEVIER

Engineering Analysis with Boundary Elements 23 (1999) 67–76

ENGINEERING ANALYSIS *with* BOUNDARY ELEMENTS

# A BEM analysis of fracture mechanics in 2D anisotropic piezoelectric solids

Ernian Pan*

*Department of Civil Engineering and Department of Mechanical Engineering, Center for Acoustics, Mechanics and Materials, University of Colorado at Boulder, Boulder, CO 80309, USA*

**Abstract**

This paper presents a single-domain boundary element method (BEM) analysis of fracture mechanics in 2D anisotropic piezoelectric solids. In this analysis, the extended displacement (elastic displacement and electrical potential) and extended traction (elastic traction and electrical displacement) integral equations are collocated on the outside boundary (no-crack boundary) of the problem and on one side of the crack surface, respectively. The Green's functions for the anisotropic piezoelectric solids in an infinite plane, a half plane, and two joined dissimilar half-planes are also derived using the complex variable function method. The extrapolation of the extended relative crack displacement is employed to calculate the extended 'stress intensity factors' (SIFs), i.e., $K_{\mathrm{I}}$, $K_{\mathrm{II}}$, $K_{\mathrm{III}}$ and $K_{\mathrm{IV}}$. For a finite crack in an infinite anisotropic piezoelectric solid, the extended SIFs obtained with the current numerical formulation were found to be very close to the exact solutions. For a central and inclined crack in a finite and anisotropic piezoelectric solid, we found that both the coupled and uncoupled (i.e., the piezoelectric coefficient $e_{ijk} = 0$) cases predict very similar stress intensity factors $K_{\mathrm{I}}$ and $K_{\mathrm{II}}$ when a uniform tension $\sigma_{yy}$ is applied, and very similar electric displacement intensity factor $K_{\mathrm{IV}}$ when a uniform electrical displacement $D_y$ is applied. However, the relative crack displacement and electrical potential along the crack surface are quite different for the coupled and uncoupled cases. Furthermore, for a inclined crack within a finite domain, we found that while a uniform $\sigma_{yy}$ ($=1\ \mathrm{N\,m^{-2}}$) induces only a very small electrical displacement intensity factor (in the unit of $\mathrm{Cm^{-3/2}}$), a uniform $D_y$ ($=1\ \mathrm{C\,m^{-2}}$) can produce very large stress intensity factors (in the unit of $\mathrm{Nm^{-3/2}}$).


*Keywords:* Boundary element method; Dual BEM; Anisotropic piezoelectric solid; General Green's functions; Fracture mechanics

## 1. Introduction

Because of their inherent coupling between electric and mechanical behavior, piezoelectric materials have found wide technological applications as transducers, sensors and actuators. Applications of piezoelectric materials as electro-mechanical devices have also stimulated a wide range of analytical researches. These include studies of electromechanical properties [1,2], analysis of fracture problems in piezoelectric materials [3–9], and solutions of laminated piezoelectric systems [10–15]. Numerical methods, such as the finite element method [16] and the boundary element method (BEM) [17] have also been applied to the analysis of electromechanical coupling under complicated conditions.

The BEM is particularly suited to cases where better accuracy is required due to problems such as stress concentrations or where the domain of interest extends to infinity. The most important feature of the BEM is that it only requires discretization of the boundary rather than the domain. Although the BEM has been applied to various branches of science and engineering, modeling of piezoelectric problems with this method is very limited [17–19]. To the author's best knowledge, there is no BEM analysis of fracture mechanics problems in anisotropic piezoelectric solids.

In this paper, we present a single-domain BEM analysis of fracture mechanics problems in anisotropic piezoelectric solids. In our approach, the extended displacement (elastic displacement and electrical potential) integral equation is applied to the outside boundary (no-crack boundary) of the problem, and the extended traction (elastic traction and electrical displacement) integral equation is applied to one side of the crack surface. These integral equations are derived from an extended reciprocal theorem. Green's functions for the 2D anisotropic piezoelectric solids in an infinite plane, a half plane and two joined dissimilar half-planes are

* Tel.: +1-303-492-7636; Fax: +1-303-492-7317; E-mail: pane@spot.colorado.edu

0955-7997/99/$ - see front matter 
PII: S0955-7997(98)00062-9

derived using the complex variable function method. In order to calculate the extended 'stress intensity factors' (SIFs), i.e., $K_{\mathrm{I}}$, $K_{\mathrm{II}}$, $K_{\mathrm{III}}$ and $K_{\mathrm{IV}}$, an extrapolation of the extended crack-tip displacement is employed. Numerical examples are carried out to show the accuracy and efficiency of the current method. Results also show that the electro-mechanical coupling can have great influence on the elastic and electric quantities and on the extended SIFs.

## 2. Basic equations

Under the condition of a static deformation, the field equations for a linear and generally anisotropic piezoelectric solid consist of [2,5,17,20]:

### 2.1. Equilibrium equations

$$\sigma_{ji,j} + F_i = 0, \qquad D_{i,i} - Q = 0, \tag{1}$$

where $\sigma_{ij}$ and $D_i$ are the stress and electric displacement, respectively; $F_i$ and $Q$ are the body force and electric charge, respectively. In this and the next sections, summation from 1 to 3 (1 to 4) over repeated lowercase (uppercase) subscripts is assumed. A subscript comma denotes the partial differentiation.

### 2.2. Constitutive relations

$$\sigma_{ij} = C_{ijlm}\gamma_{lm} - e_{kji}E_k, \qquad D_i = e_{ijk}\gamma_{jk} + \varepsilon_{ij}E_j, \tag{2}$$

where $\gamma_{ij}$ is the strain and $E_i$ is the electric field; $C_{ijlm}$, $e_{ijk}$ and $\varepsilon_{ij}$ are the elastic moduli (measured at a constant electric field), the piezoelectric coefficients (measured at a constant strain or electric field) and the dielectric constants (measured at a constant strain), respectively. It is noteworthy from Eq. (2) that the elastic and electric fields are usually coupled together. However, uncoupled solutions can be obtained by simply letting $e_{ijk} = 0$.

### 2.3. Elastic strain-displacement and electric field-potential relations

$$\gamma_{ij} = \frac{1}{2}(u_{i,j} + u_{j,i}), \qquad E_i = -\phi_{,i}, \tag{3}$$

where $u_i$ and $\phi$ are the elastic displacement and electric potential, respectively.

As in Dunn and Taya [2], we adopt the notation introduced by Barnett and Lothe [21] for the analysis of piezoelectric problems. With this notation, the elastic displacement and electric potential, the elastic strain and electric field, the stress and electric displacement, and the elastic and electric moduli (or coefficients) can be grouped together as:

$$u_I = \begin{cases} u_i, & I = 1,2,3, \\ \phi, & I = 4, \end{cases} \tag{4}$$

$$\gamma_{Ij} = \begin{cases} \gamma_{ij}, & I = 1,2,3, \\ -E_j, & I = 4, \end{cases} \tag{5}$$

$$\sigma_{iJ} = \begin{cases} \sigma_{ij}, & J = 1,2,3, \\ D_i, & J = 4, \end{cases} \tag{6}$$

$$C_{iJKl} = \begin{cases} C_{ijkl}, & J,K = 1,2,3, \\ e_{lij}, & J = 1,2,3;\ K = 4, \\ e_{ikl}, & J = 4;\ K = 1,2,3, \\ -\varepsilon_{il}, & J,K = 4. \end{cases} \tag{7}$$

In this definition, the lowercase and uppercase subscripts take on the range of 1–3 and 1–4, respectively. It is also noted that we have kept the original symbols instead of introducing new ones since they can be easily distinguished by their subscript's range. In terms of this shorthand notation, the constitutive relations can be unified into the single equation:

$$\sigma_{iJ} = C_{iJKl}\gamma_{Kl}. \tag{8}$$

Similarly, the equilibrium equations in terms of *the extended stresses* can be recast into

$$\sigma_{iJ,i} + F_J = 0, \tag{9}$$

with $F_J$ being defined as

$$F_J = \begin{cases} F_j, & J = 1,2,3, \\ -Q, & J = 4. \end{cases} \tag{10}$$

In the following sections, we will use *the extended displacement* to stand for the elastic displacement and electric potential as defined in Eq. (4), and use *the extended stress* for the stress and electric displacement as defined in Eq. (6).

## 3. BEM formulation for 2D cracked anisotropic piezoelectric solids

For a linear piezoelectric medium, one can show that the following reciprocal property of Betti type holds:

$$\sigma^{(1)}_{iJ}\gamma^{(2)}_{Ji} = \sigma^{(2)}_{iJ}\gamma^{(1)}_{Ji}, \tag{11}$$

where superscripts (1) and (2) denote two independent systems of field quantities. Integrating both sides of Eq. (11) with respect to the domain and making use of the divergence theorem, we arrive at the following integral relation:

$$\int T^{(1)}_I u^{(2)}_I \,\mathrm{d}S - \int \sigma^{(1)}_{jI,j} u^{(2)}_I \,\mathrm{d}V = \int T^{(2)}_I u^{(1)}_I \,\mathrm{d}S - \int \sigma^{(2)}_{jI,j} u^{(1)}_I \,\mathrm{d}V, \tag{12}$$

where d$S$ and d$V$ are the boundary and domain elements,

respectively, and $T_I$ is *the extended traction vector* defined by

$$T_I = \begin{cases} T_i \equiv \sum_{j=1}^{2} \sigma_{ji} n_j, & I = 1,2,3, \\ D_n \equiv \sum_{j=1}^{2} D_j n_j, & I = 4. \end{cases} \tag{13}$$

Let one of the systems correspond to the Green's function solution, and the other to the real problem, the integral relation (12) can be reduced to the integral equation:

$$u_I(\mathbf{X}_p) + \int_S T^*_{IJ}(\mathbf{X}_\mathrm{p}, \mathbf{X}_S) u_J(\mathbf{X}_S)\, \mathrm{d}S(\mathbf{X}_S)$$

$$= \int_S U^*_{IJ}(\mathbf{X}_\mathrm{p}, \mathbf{X}_S) T_J(\mathbf{X}_S)\, \mathrm{d}S(\mathbf{X}_S)$$

$$+ \int_V U^*_{IJ}(\mathbf{X}_\mathrm{p}, \mathbf{X}_S) F_J(\mathbf{X}_S)\, \mathrm{d}V(\mathbf{X}_S) \tag{14}$$

where $\mathbf{X}_\mathrm{p}$ is an arbitrary point within the domain; $U^*_{IJ}$ and $T^*_{IJ}$ are the *extended* Green's displacements and tractions derived in Appendix A.

Assuming that we can find the particular solution for a given extended body force, the domain integral in Eq. (14) can then be avoided [22]. First, we express by superposition the total extended displacements, stresses, and tractions as follows

$$u^\mathrm{t}_I = u^\mathrm{h}_I + u^\mathrm{p}_I; \qquad \sigma^\mathrm{t}_{iJ} = \sigma^\mathrm{h}_{iJ} + \sigma^\mathrm{p}_{iJ}; \qquad T^\mathrm{t}_I = T^\mathrm{h}_I + T^\mathrm{p}_I, \tag{15}$$

where the superscript 't' denotes the total solution, 'h' the homogeneous solution, and 'p' a particular solution corresponding to the extended body force and/or the extended far-field stress. Then, we substitute Eq. (15) into Eq. (14) and take into account of the crack surface. After some mathematical manipulation, we found that the total extended displacement can be expressed by the integral:

$$u^\mathrm{t}_I(\mathbf{X}_\mathrm{p}) + \int_S T^*_{IJ}(\mathbf{X}_\mathrm{p}, \mathbf{X}_S) u^\mathrm{t}_J(\mathbf{X}_S)\, \mathrm{d}S(\mathbf{X}_S)$$

$$+ \int_\Gamma T^*_{IJ}(\mathbf{X}_\mathrm{p}, \mathbf{X}_{\Gamma+})[u^\mathrm{t}_J(\mathbf{X}_{\Gamma+}) - u^\mathrm{t}_J(\mathbf{X}_{\Gamma-})]\, \mathrm{d}\Gamma(\mathbf{X}_{\Gamma+})$$

$$= \int_S U^*_{IJ}(\mathbf{X}_\mathrm{p}, \mathbf{X}_S) T^\mathrm{t}_J(\mathbf{X}_S)\, \mathrm{d}S(\mathbf{X}_S) + \int_S T^*_{IJ}(\mathbf{X}_\mathrm{p}, \mathbf{X}_S)(u^\mathrm{p}_J(\mathbf{X}_S)$$

$$- u^\mathrm{p}_I(\mathbf{X}_\mathrm{p}))\, \mathrm{d}S(\mathbf{X}_S) - \int_S U^*_{IJ}(\mathbf{X}_\mathrm{p}, \mathbf{X}_S) T^\mathrm{p}_J(\mathbf{X}_S)\, \mathrm{d}S(\mathbf{X}_S), \tag{16}$$

where $\mathrm{d}S$ and $\mathrm{d}\Gamma$ are the line elements on the no-crack boundary and crack surface, respectively, with the corresponding points being distinguished by subscripts $S$ and $\Gamma$; A point on the positive (or negative) side of the crack is denoted by $\mathbf{X}_{\Gamma+}$ (or $\mathbf{X}_{\Gamma-}$); We add that, in deriving Eq. (16), we have assumed that the extended tractions on the two sides of a crack are equal and opposite.

Let $\mathbf{X}_\mathrm{p}$ approach a point $\mathbf{Y}_S$ on the no-crack boundary, one arrives at the following boundary integral equation

$$b_{IJ} u^\mathrm{t}_J(\mathbf{Y}_S) + \fint_S T^*_{IJ}(\mathbf{Y}_S, \mathbf{X}_S) u^\mathrm{t}_J(\mathbf{X}_S)\, \mathrm{d}S(\mathbf{X}_S)$$

$$+ \int_\Gamma T^*_{IJ}(\mathbf{Y}_S, \mathbf{X}_{\Gamma+})[u^\mathrm{t}_J(\mathbf{X}_{\Gamma+}) - u^\mathrm{t}_J(\mathbf{X}_{\Gamma-})]\, \mathrm{d}\Gamma(\mathbf{X}_{\Gamma+})$$

$$= \int_S U^*_{IJ}(\mathbf{Y}_S, \mathbf{X}_S) T^\mathrm{t}_J(\mathbf{X}_S)\, \mathrm{d}S(\mathbf{X}_S) + \int_S T^*_{IJ}(\mathbf{Y}_S, \mathbf{X}_S)(u^\mathrm{p}_J(\mathbf{X}_S)$$

$$- u^\mathrm{p}_I(\mathbf{Y}_S))\, \mathrm{d}S(\mathbf{X}_S) - \int_S U^*_{IJ}(\mathbf{Y}_S, \mathbf{X}_S) T^\mathrm{p}_J(\mathbf{X}_S)\, \mathrm{d}S(\mathbf{X}_S), \tag{17}$$

where $b_{IJ}$ are coefficients that depend only upon the local geometry of the no-crack boundary at $\mathbf{Y}_S$.

It is observed that all the terms on the right-hand side of Eq. (17) have only weak singularities, thus, are integrable. Although the second term on the left-hand side of Eq. (17) has a strong singularity, it can be treated by the rigid body motion method (i.e., $u_I$ = constant throughout the whole domain). At the same time, the calculation of $b_{IJ}$ can also be avoided.

For the uncracked case, Eq. (17) can be applied to solve the extended displacement and stress in a 2D general anisotropic and piezoelectric domain with the crack surface integral term being omitted. It is well known, however, that for a cracked domain, Eq. (17) does not have a unique solution [23]. For this situation, the traction integral equation of Pan and Amadei [24] can be employed and extended to the piezoelectric case. Assume that $\mathbf{Y}_\Gamma$ is a smooth point on the crack surface, the extended traction integral equation can be derived as

$$0.5[T^\mathrm{t}_M(\mathbf{Y}_{\Gamma+}) - T^\mathrm{t}_M(\mathbf{Y}_{\Gamma-})] + n_l(\mathbf{Y}_{\Gamma+})$$

$$\times \int_S C_{lMIk} T^*_{IJ,k}(\mathbf{Y}_{\Gamma+}, \mathbf{X}_S) u^\mathrm{t}_J(\mathbf{X}_S)\, \mathrm{d}S(\mathbf{X}_S)$$

$$+ n_l(\mathbf{Y}_{\Gamma+}) \fint_\Gamma C_{lMIk} T^*_{IJ,k}(\mathbf{Y}_{\Gamma+}, \mathbf{X}_{\Gamma+})[u^\mathrm{t}_J(\mathbf{X}_{\Gamma+})$$

$$- u^\mathrm{t}_J(\mathbf{X}_{\Gamma-})]\, \mathrm{d}\Gamma(\mathbf{X}_{\Gamma+}) = 0.5[T^\mathrm{p}_M(\mathbf{Y}_{\Gamma+}) - T^\mathrm{p}_M(\mathbf{Y}_{\Gamma-})]$$

$$+ n_l(\mathbf{Y}_{\Gamma+}) \int_S C_{lMIk} U^*_{IJ,k}(\mathbf{Y}_{\Gamma+}, \mathbf{X}_S) T^\mathrm{t}_J(\mathbf{X}_S)\, \mathrm{d}S(\mathbf{X}_S)$$

$$+ n_l(\mathbf{Y}_{\Gamma+}) \int_S C_{lMIk} T^*_{IJ,k}(\mathbf{Y}_{\Gamma+}, \mathbf{X}_S) u^\mathrm{p}_J(\mathbf{X}_S)\, \mathrm{d}S(\mathbf{X}_S)$$

$$- n_l(\mathbf{Y}_{\Gamma+}) \int_S C_{lMIk} U^*_{IJ,k}(\mathbf{Y}_{\Gamma+}, \mathbf{X}_S) T^\mathrm{p}_J(\mathbf{X}_S)\, \mathrm{d}S(\mathbf{X}_S), \tag{18}$$

where $n_l$ is the outward normal at the crack surface $\mathbf{Y}_{\Gamma+}$ and $C_{lMIk}$ is the extended stiffness tensor defined in Eq. (7).

Eqs. (17) and (18) form a new pair of boundary integral equations and they are the extension of the existing single-domain BEM formulation [24–26] to the anisotropic piezoelectric medium. In this new formulation, the extended displacement integral equation is collocated on the no-crack boundary, and the extended traction integral equation on one side of the crack surface. The effect of the extended body force and/or the extended far-field stress have been included by superposing the corresponding particular solution, which makes the problem very similar to the one associated with the homogeneous governing equation. The only difference is that for the extended body force and/or the extended far-field stress cases, two extra integral terms related to the particular solution need to be added to the homogeneous integral equations. The advantage of using Eqs. (17) and (18) is that for the extended far-field stress case, the artificial truncation of the infinite domain or transferring of the extended far-field stress onto the problem boundary can be avoided. While the former method increases the size of the problem and also introduces errors because of the truncation of the region, the latter may not be suitable for cases where the boundary has a complex shape. It is also worth mentioning that for problems containing crack surfaces only, i.e., cracks in an infinite, a half plane or in two bonded half planes, only Eq. (18) is required with the no-crack boundary integral terms being omitted.

The boundary integral Eqs. (17) and (18) can be discretized and solved numerically for the unknown extended boundary displacements (or extended displacement discontinuities on the crack surface) and extended tractions. The hypersingular integral term in Eq. (18) is handled by an accurate and efficient Gauss quadrature formulae [24,27], which is similar to the traditional weighted Gauss quadrature but with a different weight.

## 4. Crack tip modeling and calculation of the extended SIFs

In order to capture the square root characteristics of the extended relative crack displacement (ERCD) near the crack-tip, we construct the following crack-tip element with its tip at $s=-1$:

$$\Delta u_I = \sum_{k=1}^{3} \phi_k \Delta u_I^k, \tag{19}$$

where the subscript $I$ (=1,2,3,4) denotes the components of the ERCD, and the superscript $k$ (=1,2,3) denotes the ERCD at nodes $s=-2/3,0,2/3$, respectively. The shape functions $\phi_k$ are [26]

$$\phi_1 = \frac{3\sqrt{3}}{8}\sqrt{s+1}[5-8(s+1)+3(s+1)^2],$$

$$\phi_2 = \frac{1}{4}\sqrt{s+1}[-5+18(s+1)-9(s+1)^2],$$

$$\phi_3 = \frac{3\sqrt{3}}{8\sqrt{5}}\sqrt{s+1}[1-4(s+1)+3(s+1)^2]. \tag{20}$$

For the extended SIF calculation, we employ the extrapolation method of the ERCDs, which requires an analytical relation between the extended displacement and the extended SIFs. This relation can be expressed as [5]:

$$\Delta\mathbf{u}(r) = 2\sqrt{\frac{2r}{\pi}}\mathbf{Y}\mathbf{K}, \tag{21}$$

where the matrix $\mathbf{Y}$ is given in Eq. (A9) of Appendix A and $\mathbf{K}$ is the extended SIF vector defined as

$$\mathbf{K} = \{K_{\mathrm{II}}, K_{\mathrm{I}}, K_{\mathrm{III}}, K_{\mathrm{IV}}\}^{\mathrm{t}} \tag{22}$$

with $K_{\mathrm{I}}$, $K_{\mathrm{II}}$ and $K_{\mathrm{III}}$ being the usual stress intensity factors and $K_{\mathrm{IV}}$ being the electrical displacement intensity factor.

On the crack-tip element, equating the ERCDs from the numerical calculation (19) to the analytical expression (21), one then obtains a set of algebraic equations from which the extended SIFs can be solved.

## 5. Numerical examples

The piezoelectric material chosen for the numerical examples is lead zirconate titanate (PZT-4) ceramic [2]. The material constants of PZT-4 are given in Table 1 in which, the elastic constants $C_{ij}$ are in $10^9$ N m$^{-2}$, the piezoelectric coefficient $e_{ij}$ in C m$^{-2}$, and the dielectric constants $\varepsilon_{ij}$ in $10^{-9}$ C/(Vm). The axis of symmetry of this transversely isotropic PZT-4 is along the $y$-axis.

Table 1
Electroelastic moduli of the PZT-4 material

| $C_{11}$ | $C_{12}$ | $C_{13}$ | $C_{22}$ | $C_{44}$ | $C_{55}=0.5(C_{11}-C_{13})$ |
|---|---|---|---|---|---|
| 139 | 74.3 | 77.8 | 115 | 25.6 | 30.6 |
| $e_{21}$ | $e_{22}$ | $e_{16}$ | | $\varepsilon_{11}$ | $\varepsilon_{22}$ |
| −5.2 | 15.1 | 12.7 | | 6.461 | 5.620 |

The first example corresponds to a finite and horizontal crack along the $x$-direction in an infinite PZT-4 medium under a uniform far-field stress or electric displacement. We used 20 discontinuous quadratic elements to discretize the crack surface which has a length of $2a$ (=1 m). The normalized extended SIFs obtained with the current BEM

Table 2
Normalized extended SIFs for a horizontal crack in an infinite domain

| | $K_{\mathrm{I}}/\sigma_{yy}\sqrt{\pi a}$ | $K_{\mathrm{II}}/\sigma_{xy}\sqrt{\pi a}$ | $K_{\mathrm{III}}/\sigma_{yz}\sqrt{\pi a}$ | $K_{\mathrm{IV}}/D_{y}\sqrt{\pi a}$ |
|---|---|---|---|---|
| Numerical | 0.9994 | 0.9994 | 0.9994 | 0.9994 |
| Exact | 1.0000 | 1.0000 | 1.0000 | 1.0000 |

Table 3
Relative crack displacement and electric potential caused by a far-field $\sigma_{yy}(=1\ \mathrm{N/m^2})$

| | $\Delta u_y$ ($10^{-12}$ m) | | $\Delta\phi$ ($10^{-1}$ V) | |
|---|---|---|---|---|
| $x$ (m) | Numerical | Exact | Numerical | Exact |
| 0.492 | 0.032 | 0.032 | 0.040 | 0.040 |
| 0.425 | 0.094 | 0.093 | 0.116 | 0.116 |
| 0.358 | 0.124 | 0.124 | 0.154 | 0.154 |
| 0.292 | 0.144 | 0.144 | 0.179 | 0.179 |
| 0.225 | 0.158 | 0.158 | 0.197 | 0.197 |
| 0.158 | 0.168 | 0.168 | 0.210 | 0.210 |
| 0.092 | 0.174 | 0.174 | 0.217 | 0.217 |
| 0.025 | 0.177 | 0.177 | 0.221 | 0.221 |

formulation are listed in Table 2 and compared to the exact closed-form solutions [3–5]. It is obvious that very accurate SIFs can be obtained by the proposed formulation.

It is interesting to note that even though the extended SIFs are uncoupled (i.e., a far-field stress induces the stress intensity factors only, and a far-field electric displacement induces the electric displacement intensity factor only), the ERCDs are usually coupled together. For example, Tables 3 and 4 give the relative crack displacement and electric potential caused by a far-field stress $\sigma_{yy}$ and a far-field electrical displacement $D_y$. It is obvious that a far-field stress induces a non-zero $\Delta\phi$ even though the corresponding $K_{\mathrm{IV}}$ is zero. Similarly, a far-field electrical displacement can induce a non-zero $\Delta u_y$ even though the corresponding $K_{\mathrm{II}}$ is zero. The exact closed-form solutions [5] are also given in Tables 3 and 4, which show that the present numerical method is very accurate. Finally, we noticed from Tables 3 and 4 that the value of $\Delta\phi$ ($10^{-1}$ V) caused by a far-field stress $\sigma_{yy}$ is identical to that of $\Delta u_y$ ($10^{-1}$ m) caused by a far-field electric displacement $D_y$, a consequence of the Betti-type reciprocity.

The second example also corresponds to a finite crack in an infinite PZT-4 medium. The crack is inclined 45° to the positive $x$-direction and has a length of $2a$, which is again under a uniform far-field stress or electric displacement. The exact closed-form solution can be obtained simply by the coordinate transformation for a tensor and a vector. Here we used 10 discontinuous quadratic elements to discretize the

Table 4
Relative crack displacement and electric potential caused by a far-field $D_y$ $(=1\ \mathrm{C\,m^{-2}})$

| | $\Delta\phi$ ($10^{8}$ V) | | $\Delta u_y$ ($10^{-1}$ m) | |
|---|---|---|---|---|
| $x$ (m) | Numerical | Exact | Numerical | Exact |
| 0.492 | 0.161 | 0.160 | 0.040 | 0.040 |
| 0.425 | 0.466 | 0.465 | 0.116 | 0.116 |
| 0.358 | 0.616 | 0.616 | 0.154 | 0.154 |
| 0.292 | 0.717 | 0.717 | 0.179 | 0.179 |
| 0.225 | 0.789 | 0.789 | 0.197 | 0.197 |
| 0.158 | 0.838 | 0.838 | 0.210 | 0.210 |
| 0.092 | 0.868 | 0.868 | 0.217 | 0.217 |
| 0.025 | 0.882 | 0.882 | 0.221 | 0.221 |

Table 5
Normalized extended SIFs for an inclined crack in an infinite domain

| | $K_{\mathrm{I}}/\sigma_{yy}\sqrt{\pi a}$ | $K_{\mathrm{II}}/\sigma_{yy}\sqrt{\pi a}$ | $K_{\mathrm{I}}/\sigma_{xy}\sqrt{\pi a}$ | $K_{\mathrm{III}}/\sigma_{yz}\sqrt{\pi a}$ | $K_{\mathrm{IV}}/D_y\sqrt{\pi a}$ |
|---|---|---|---|---|---|
| Numerical | 0.4968 | 0.4968 | −0.9937 | 0.7108 | 0.7108 |
| Exact | 0.5000 | 0.5000 | −1.0000 | 0.7071 | 0.7071 |

crack surface. Our numerical results of the normalized extended SIFs are listed in Table 5 and compared to the exact closed-form solutions. Again, excellent agreement is obtained.

As a third and final example, a finite, rectangular, and PZT-4 solid with a central crack inclined 45° to the horizontal direction is considered (Fig. 1). A uniform tension or electric displacement is applied in the $y$-direction. The ratios of crack length to width, and of height to width are $a/w = 0.2$ and $h/w = 2.0$, respectively (in dimension, $w = 0.5$ m, $h = 1$ m, $a = 0.1$ m). We used 10 discontinuous quadratic elements on the crack surface and 32 quadratic elements on the outside boundaries. While Tables 6 and 7 give the results of the normalized extended SIFs for both the coupled and uncoupled ($e_{ijk} = 0$) cases when the uniform $\sigma_{yy}$ and $D_y$ are applied, Tables 8 and 9 list the corresponding relative crack displacement and electric potential. In Table 6, $D^*$ is a nominal electric displacement in the unit of $\mathrm{C\,m^{-2}}$ with its amplitude equal to that of $\sigma_{yy}$ in the unit of $\mathrm{N\,m^{-2}}$, and in Table 7, $\sigma^*$ is a nominal stress in the unit of $\mathrm{N\,m^{-2}}$ with its amplitude equal to that of $D_y$ in the unit of $\mathrm{C\,m^{-2}}$. Several observations can be made from those tables: (1) Table 6 indicates that when the uniform tension $\sigma_{yy}$ is applied, both the coupled and uncoupled cases predict very similar values for the normalized $K_{\mathrm{I}}/\sigma_{yy}\sqrt{\pi a}$ and $K_{\mathrm{II}}/\sigma_{yy}\sqrt{\pi a}$. Similarly, Table 7 shows that when the uniform electric displacement $D_y$ is applied, the values of the normalized $K_{\mathrm{IV}}/D_y\sqrt{\pi a}$ for both the coupled and uncoupled cases are very close to each other. (2) It is noted that even though the extended SIFs are not affected much by the electromechanical coupling, the relative crack quantities (relative

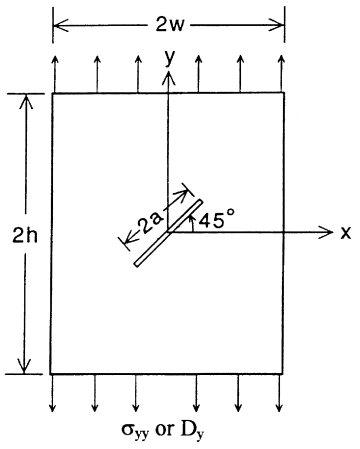


Fig. 1. An anisotropic, piezoelectric, and finite rectangular solid with a central crack inclined 45° to the horizontal direction under a uniform tension or electric displacement in the $y$-direction.

Table 6
Normalized extended SIFs for an inclined crack in a finite solid under $\sigma_{yy}$ ($=1$ N m$^{-2}$)

| | $K_I/\sigma_{yy}\sqrt{\pi a}$ | $K_{II}/\sigma_{yy}\sqrt{\pi a}$ | $K_{IV}/D^*\sqrt{\pi a}$ |
|---|---|---|---|
| Coupled | 0.5303 | 0.5151 | $-2.97 \times 10^{-12}$ |
| Uncoupled | 0.5275 | 0.5151 | 0.0000 |

crack displacement and electric potential) are quite different for the coupled and uncoupled cases. This can be observed in Table 8 for $\Delta u_x$ and $\Delta u_y$, and in Table 9 for $\Delta\varphi$. (3) It is also interesting to note from both Tables 6 and 7 that for the coupled case, while a uniform $\sigma_{yy}$ ($=1$ N m$^{-2}$) induces only a very small electric displacement intensity factor (in the unit of Cm$^{-3/2}$), a uniform $D_y$ ($=1$ C m$^{-2}$) can produce very large stress intensity factors (in the unit of Nm$^{-3/2}$). This phenomenon indicates clearly that the crack initiation criteria based on a single SIF (for the elastic case) cannot be simply extended to the piezoelectric case. Instead, the energy-based criteria, which include the contribution of each component of the extended SIFs, should be employed. (4) The Betti-type reciprocity is shown again in Tables 8 and 9 where $\Delta\phi$ ($10^{-2}$ V) induced by the uniform tension $\sigma_{yy}$ is equal to $\Delta u_y$ ($10^{-2}$ m) induced by the uniform electric displacement $D_y$.

## 6. Conclusions

A single-domain BEM formulation has been proposed for fracture mechanics analysis in cracked 2D anisotropic piezoelectric solids. In this approach, the extended displacements (elastic displacement and electric potential) are collocated on the no-crack boundary and the extended traction (elastic traction and electric displacement) on one side of the crack surface. This work is an extension of the existing single-domain BEM formulation [24–26] to the anisotropic piezoelectric solid. The Green's functions for a general anisotropic piezoelectric solid in an infinite plane, a half-plane and two joined dissimilar half-planes have been derived using the complex variable function method. Numerical examples for the calculation of the extended SIFs are also carried out. For a finite crack in an infinite and anisotropic piezoelectric medium, the extended SIFs obtained with the current numerical method were found to be very close to the exact solutions. For an inclined and central crack in a finite piezoelectric solid, we found that

Table 7
Normalized extended SIFs for an inclined crack in a finite solid under $D_y$ ($=1$ C m$^{-2}$)

| | $K_{IV}/D_y\sqrt{\pi a}$ | $K_I/\sigma^*\sqrt{\pi a}$ | $K_{II}/\sigma^*\sqrt{\pi a}$ |
|---|---|---|---|
| Coupled | −0.72785 | $-1.417 \times 10^6$ | $1.692 \times 10^5$ |
| Uncoupled | −0.72776 | 0.0000 | 0.0000 |

Table 8
Relative crack displacement and electric potential caused by $\sigma_{yy}$ ($=1$ N m$^{-2}$)

| | Coupled | | | Uncoupled | |
|---|---|---|---|---|---|
| $x = y$ ($10^{-1}$ m) | $\Delta u_x$ ($10^{-13}$ m) | $\Delta u_y$ ($10^{-11}$ m) | $\Delta\phi$ ($10^{-2}$ V)[a] | $\Delta u_x$ ($10^{-13}$ m) | $\Delta u_y$ ($10^{-11}$ m) |
| 0.684 | 0.099 | − 0.066 | 0.081 | 0.102 | − 0.095 |
| 0.589 | 0.216 | − 0.143 | 0.175 | 0.223 | − 0.205 |
| 0.495 | 0.283 | − 0.185 | 0.226 | 0.292 | − 0.265 |
| 0.401 | 0.330 | − 0.214 | 0.261 | 0.340 | − 0.305 |
| 0.306 | 0.365 | − 0.234 | 0.285 | 0.375 | − 0.334 |
| 0.212 | 0.388 | − 0.247 | 0.302 | 0.400 | − 0.353 |
| 0.118 | 0.403 | − 0.256 | 0.312 | 0.415 | − 0.365 |
| 0.024 | 0.409 | − 0.259 | 0.316 | 0.421 | − 0.370 |

[a] $\Delta\phi$ is zero for the uncoupled case.

Table 9
Relative crack displacement and electric potential caused by $D_y$ ($=1$ C m$^{-2}$)

| | Coupled | | | Uncoupled |
|---|---|---|---|---|
| $x = y$ ($10^{-1}$ m) | $\Delta u_x$ ($10^{-5}$ m)[a] | $\Delta u_y$ ($10^{-2}$ m)[a] | $\Delta\phi$ ($10^8$ V) | $\Delta\phi$ ($10^8$ V) |
| 0.684 | 0.103 | 0.081 | 0.032 | 0.061 |
| 0.589 | 0.226 | 0.175 | 0.070 | 0.132 |
| 0.495 | 0.296 | 0.226 | 0.090 | 0.170 |
| 0.401 | 0.346 | 0.261 | 0.104 | 0.196 |
| 0.306 | 0.382 | 0.285 | 0.114 | 0.214 |
| 0.212 | 0.407 | 0.302 | 0.121 | 0.227 |
| 0.118 | 0.422 | 0.312 | 0.125 | 0.234 |
| 0.024 | 0.429 | 0.316 | 0.127 | 0.238 |

[a] $\Delta u_x$ and $\Delta u_y$ are zero for the uncoupled case.

both the coupled and uncoupled ($e_{ijk} = 0$) cases predict very similar stress intensity factors $K_I$ and $K_{II}$ when a uniform tension is applied, and very similar electric displacement intensity factor $K_{IV}$ when a uniform electrical displacement is applied. However, the relative crack displacements and electric potentials along the crack are quite different for the coupled and uncoupled cases. Furthermore, for the coupled case, while a uniform $\sigma_{yy}$ ($=1$ N m$^{-2}$) induces only a very small electrical displacement intensity factor (in the unit of Cm$^{-3/2}$), a uniform $D_y$ ($=1$ C m$^{-2}$) can produce very large stress intensity factors (in the unit of Nm$^{-3/2}$). This phenomenon is new to the author and it may shed a new light on the future development of fracture mechanics analysis for piezoelectric solids.

## Acknowledgements

The author would like to thank Prof. Martin L. Dunn in the Department of Mechanical Engineering for stimulating and constructive discussions. This work is supported by National Science Foundation under Grants CMS-9622645 and CMS-9713559.

## Appendix A

In this appendix, the Green's functions for anisotropic piezoelectric solids in an infinite plane, a half-plane and two-jointed dissimilar half-planes are derived. Previously, Lee and Jiang [18] using the Fourier transform method derived the Green's functions of transversely isotropic piezoelectric solids in an infinite plane. Sosa and Castro [28] using a state space approach combined with the Fourier transform obtained the Green's functions due to a compressive point force or a point charge acting on the surface of a transversely isotropic piezoelectric half plane. When a piezoelectric material possesses lower symmetry, neither the infinite-plane nor the half-plane Green's function is available.

For a 2D, anisotropic and linear piezoelectric medium, the extended displacement and stress can be described with four complex functions $f_I(z_I)$ [5,29]

$$u_I = 2\,\mathrm{Re}\left[\sum_{J=1}^{4} A_{IJ} f_J(z_J)\right], \qquad \sigma_{2I} = 2\,\mathrm{Re}\left[\sum_{J=1}^{4} B_{IJ} f_J'(z_J)\right],$$

$$\sigma_{1I} = -2\,\mathrm{Re}\left[\sum_{J=1}^{4} B_{IJ}\mu_J f_J'(z_J)\right],$$

$$\phi_I = -2\,\mathrm{Re}\left[\sum_{J=1}^{4} B_{IJ} f_J(z_J)\right]. \tag{A.1}$$

In the last equation, $\phi_I$ is *the extended resultant traction* on a curve, i.e., the integral of *the extended traction* defined by

$$T_I = \begin{cases} T_i \equiv \sum_{j=1}^{2} \sigma_{ji} n_j, & I = 1,2,3, \\ D_n \equiv \sum_{j=1}^{2} D_j n_j, & I = 4, \end{cases} \tag{A.2}$$

with $n_j$ ($j = 1,2$) being the unit outward normal of the curve.

In Eq. (A.1), $z_J = x + \mu_J y$; Re denotes the real part of a complex variable or function; a prime denotes the derivative; and $\mu_J$ ($J = 1,2,3,4$) are four distinct complex roots with positive imaginary part of the following equation

$$\left|C_{1IJ1} + \mu(C_{1IJ2} + C_{1JI2}) + \mu^2 C_{2IJ2}\right| = 0 \tag{A.3}$$

For each of the characteristic roots $\mu_K$, each column of the matrix **A** in Eq. (A.1) is the eigenvector of the following equation:

$$\sum_{J=1}^{4} \left[C_{1IJ1} + \mu_K(C_{1IJ2} + C_{1JI2}) + \mu_K^2 C_{2IJ2}\right] A_{JK} = 0. \tag{A.4}$$

Once the matrix **A** is found, the matrix **B** in Eq. (A.1) can be obtained by

$$B_{IK} = \sum_{J=1}^{4} \left(C_{1JI2} + \mu_K C_{2IJ2}\right) A_{JK}. \tag{A.5}$$

It is noted that in writing the general solution (A.1), we have assumed that the eigenfunction (A.3) has eight roots, which form four conjugate pairs. This requires equally that Eq. (A.3) admits no real root which is true as proved by Suo et al. [5]. Another assumption in writing the solution (A.1) is that Eq. (A.3) has eight different eigenvalues. For an isotropic, non-piezoelectric dielectric, degenerated eigenvalues can occur. In this case, however, a quasi-isotropic material can replace the isotropic material so that the general solution (A.1) is still valid. In general, the difference between the solution based on the quasi-isotropic model and that based on the isotropic model is negligible, as has been verified by Sollero et al. [30] and Pan and Amadei [24] for the purely elastic case. It is also noted that since each column of the matrix **A** is an eigenvector, the representation of Eq. (A.1) is uniquely determined by the material properties, up to the four normalized factors of the matrix **A**.

In order to obtain the Green's functions for different domain cases, we use the one-complex-variable approach [5] and define a vector function as

$$\mathbf{f}(z) = \left[f_1(z), f_2(z), f_3(z), f_4(z)\right]^{\mathrm{t}}, \tag{A.6}$$

with the argument having the generic form $z = x + \mu y$. Once the complex vector function is obtained, the Green's functions, i.e., the extended displacement and stress fields can be derived from Eq. (A.1).

### *Appendix A.1 Green's functions in an infinite piezoelectric plane*

Assume that there is an extended dislocation $\{d_J\} = \mathbf{d} = (\mathbf{u}^+ - \mathbf{u}^-)$ and an extended force $\{p_J\} = \mathbf{p} = (\mathbf{T}^- - \mathbf{T}^+)$ acting at the source point $(x^0, y^0)$, the solution for the complex functions can be expressed as [31,32]:

$$f_J(z) = q_J \ln(z - s_J), \tag{A.7}$$

where $s_J = x^0 + \mu_J y^0$, and $\mathbf{q} = \{q_J\}$ is a complex coefficient vector. To find **q**, we substitute Eq. (A.7) into Eq. (A.1) and let the jump of the extended displacement and resultant traction be equal to **d** and **p**, respectively. This gives us the following expression for **q**

$$\mathbf{q} = \frac{1}{2\pi}[\mathbf{B}^{-1}(\mathbf{Y} + \bar{\mathbf{Y}})^{-1}\mathbf{d} - \mathbf{A}^{-1}(\mathbf{Y}^{-1} + \bar{\mathbf{Y}}^{-1})^{-1}\mathbf{p}, \tag{A.8}$$

where overbar means complex conjugate; superscript $-1$ means matrix inverse; and **Y** is given by

$$\mathbf{Y} = i\mathbf{A}\mathbf{B}^{-1} \tag{A.9}$$

with $i = \sqrt{-1}$.

If $\mathbf{d} = \mathbf{0}$, the Green's functions will be those corresponding to an extended point force only. The substitution of the complex function (A.7) in Eq. (A.1) gives the Green's extended displacement and traction. For an extended unit point force, the extended displacements are found to be

$$U_{KL}^{*} = \frac{-1}{\pi}\,\mathrm{Re}\left[\sum_{J=1}^{4} A_{LJ} H_{JK} \ln(z_J - s_J)\right]. \tag{A.10}$$

Similarly, the extended tractions can be expressed as

$$T^*_{KL} = \frac{1}{\pi}\,\mathrm{Re}\left[\sum_{J=1}^{4} B_{LJ}\,\frac{\mu_J n_x - n_y}{z_J - s_J} H_{JK}\right], \tag{A.11}$$

where

$$\mathbf{H} = \mathbf{A}^{-1}(\mathbf{Y}^{-1} + \bar{\mathbf{Y}}^{-1})^{-1}. \tag{A.12}$$

In Eqs. (A.10) and (A.11), $z_J = x + \mu_J y$ and $s_J = x^0 + \mu_J y^0$ correspond to the field and source points, respectively; $n_x$ and $n_y$ are the $x$ and $y$ components of the unit outward normal at the field point $(x,y)$.

It is noteworthy that by replacing $\mathbf{H}$ in Eqs. (A.10) and (A.11) with $-\mathbf{B}^{-1}(\mathbf{Y} + \bar{\mathbf{Y}})^{-1}$, we then obtain the Green's functions due to an extended point dislocation.

Based on an eight-dimensional formalism, Barnett and Lothe [21] derived the extended displacement in an infinite plane due to an elastic dislocation ($d_J \neq 0$ for $J = 1,2,3$; $d_4 = 0$) and an electric charge ($p_J = 0$ for $J = 1,2,3$; $p_4 \neq 0$). Using the Fourier transform, Lee and Jiang [18] obtained the Green's functions for a transversely isotropic piezoelectric infinite plane. These solutions are particular cases of Eqs. (A.10) and (A.11).

Eqs. (A.10) and (A.11) show that the Green's functions $U^*_{KL}$ and $T^*_{KL}$ for piezoelectric solids are $4 \times 4$ matrices with their first index ($K$) denoting the source components and second index ($L$) the field components. Since these Green's matrices are usually full for general anisotropic piezoelectric solids, the elastic and electric fields are coupled together. That is, a body force will induce an electric potential, and an electric charge will generate an elastic displacement. The physical meaning of the Green's matrices can be explained. Take the extended displacement $U^*_{KL}$ for example, the meaning of this $4 \times 4$ Green's function is:

1. the elastic displacement ($L = 1$–$3$) at field point $z$ due to a unit force ($K = 1$–$3$) at source point $s$;
2. the elastic displacement ($L = 1$–$3$) at field point $z$ due to a unit charge ($K = 4$) at source point $s$;
3. the electric potential ($L = 4$) at field point $z$ due to a unit force ($K = 1$–$3$) at source point $s$; and finally,
4. the electric potential ($L = 4$) at field point $z$ due to a unit charge ($K = 4$) at source point $s$.

### *Appendix A.2 Green's functions in a piezoelectric half-plane*

For a half-plane problem, we let the medium occupy the lower half-plane ($y < 0$) and let $y = 0$ correspond to the extended traction-free surface (i.e., the traction and normal component of the electric displacement are zero at $y = 0$). The source point $(x^0,y^0)$ is located anywhere within the lower half-plane ($y^0 < 0$). To find the complex functions in Eq. (A.1), we assume the following vector function expression:

$$\mathbf{f}(z) = \mathbf{f}^0(z) + \mathbf{f}^c(z), \tag{A.13}$$

where $\mathbf{f}^0(z)$ is the full-plane solution given in Eq. (A.7) and $\mathbf{f}^c(z)$ is a complementary vector function to be determined. In order to obtain $\mathbf{f}^c(z)$, we substitute $\mathbf{f}(z)$ into the extended resultant traction equation (last equation of (A.1)) and enforce the extended traction-free condition at $y = 0$. Following the standard analytical continuation of complex functions, the complementary vector function is found as

$$\mathbf{f}^c(z) = -\mathbf{B}^{-1}\bar{\mathbf{B}}\bar{\mathbf{f}}^0(z). \tag{A.14}$$

With this solved complex vector function, the Green's functions in a half-plane can then be derived from Eq. (A.1). For the extended displacement, the Green's matrix is

$$U^*_{KL} = \frac{-1}{\pi}\,\mathrm{Re}\left\{\sum_{J=1}^{4} A_{LJ}\left[H_{JK}\ln(z_J - s_J) - \sum_{I=1}^{4} W_{JI}\bar{H}_{IK}\ln(z_J - \bar{s}_I)\right]\right\}, \tag{A.15}$$

with

$$\mathbf{W} = \mathbf{B}^{-1}\bar{\mathbf{B}} \tag{A.16}$$

and for the extended traction, it is

$$T^*_{KL} = \frac{1}{\pi}\,\mathrm{Re} \times \left\{\sum_{J=1}^{4} B_{LJ}\left[\frac{\mu_J n_x - n_y}{z_J - s_J} H_{JK} - \sum_{I=1}^{4} W_{JI}\,\frac{\mu_J n_x - n_y}{z_J - \bar{s}_I}\bar{H}_{IK}\right]\right\}. \tag{A.17}$$

For a transversely isotropic piezoelectric half-plane, Sosa and Castro [28] derived the Green's solutions for a vertical point force and a point charge acting on the surface of the half-plane, which is a particular case of the current half-plane solution.

### *Appendix A.3 Green's functions in piezoelectric bimaterials*

We now assume that the medium is composed of two joined piezoelectric half-planes. We let the interface be along the $x$-axis, and the upper ($y > 0$) and lower ($y < 0$) half-planes be occupied by materials #1 and #2, respectively.

For a concentrated source acting at the point $(x^0,y^0)$ in material #2 ($y^0 < 0$), we express the complex vector function as [31]

$$\mathbf{f}(z) = \begin{cases} \mathbf{f}^{\mathrm{U}}(z), & z \in 1, \\ \mathbf{f}^{\mathrm{L}}(z) + \mathbf{f}^0_{(2)}(z), & z \in 2. \end{cases} \tag{A.18}$$

In Eq. (A.18), the vector function $\mathbf{f}^0_{(2)}$ is the infinite-plane solution given in Eq. (A.7) with piezoelectric properties of material #2. $\mathbf{f}^{\mathrm{U}}(z)$ and $\mathbf{f}^{\mathrm{L}}(z)$ are analytic in upper (material #1) and lower (material #2) half-planes, respectively. The solutions to them can be found by the requirement of the

continuities of the extended resultant traction and displacement across the interface, along with the standard analytic continuation arguments. Following this path and after some complex algebraic manipulation, the complex vector functions in materials #1 and #2 are obtained as

$$\mathbf{f}(z)=\begin{cases}\mathbf{B}_{(1)}^{-1}(\mathbf{Y}_{(1)}+\bar{\mathbf{Y}}_{(2)})^{-1}(\bar{\mathbf{Y}}_{(2)}+\mathbf{Y}_{(2)})\mathbf{B}_{(2)}\mathbf{f}_{(2)}^{0}(z), & z\in 1,\\ \mathbf{B}_{(2)}^{-1}(\bar{\mathbf{Y}}_{(1)}+\mathbf{Y}_{(2)})^{-1}(\bar{\mathbf{Y}}_{(2)}-\bar{\mathbf{Y}}_{(1)})\bar{\mathbf{B}}_{(2)}\bar{\mathbf{f}}_{(2)}^{0}(z)+\mathbf{f}_{(2)}^{0}(z), & z\in 2.\end{cases} \tag{A.19}$$

In Eq. (A.19), the special subscripts (1) and (2) are used exclusively to denote that the corresponding matrix or vector is in material #1 ($y>0$) and material #2 ($y<0$), respectively.

Similarly, for a source point in material #1 ($y^0>0$), these complex functions can be found as

$$\mathbf{f}(z)=\begin{cases}\mathbf{B}_{(1)}^{-1}(\bar{\mathbf{Y}}_{(2)}+\mathbf{Y}_{(1)})^{-1}(\bar{\mathbf{Y}}_{(1)}-\bar{\mathbf{Y}}_{(2)})\bar{\mathbf{B}}_{(1)}\bar{\mathbf{f}}_{(1)}^{0}(z)+\mathbf{f}_{(1)}^{0}(z), & z\in 1,\\ \mathbf{B}_{(2)}^{-1}(\mathbf{Y}_{(2)}+\bar{\mathbf{Y}}_{(1)})^{-1}(\bar{\mathbf{Y}}_{(1)}+\mathbf{Y}_{(1)})\mathbf{B}_{(1)}\mathbf{f}_{(1)}^{0}(z), & z\in 2,\end{cases} \tag{A.20}$$

where the vector function $\mathbf{f}_{(1)}^{0}$ is again the infinite-plane solution given in Eq. (A.7) but with piezoelectric properties of material #1.

With the complex functions giving in Eqs. (A.19) and (A.20), the Green's functions of the extended displacement and traction can be obtained by substituting these complex functions into Eq. (A.1). These Green's functions have four different forms depending on the locations of the field and source points. The complete expressions for them are given below with special superscripts and subscripts (1) and (2) being used exclusively to denote that the corresponding quantities are in materials #1 ($y>0$) and #2 ($y<0$), respectively.

(I) For source ($s$) and field ($z$) points in material #1 ($y>0$):

$$U_{KL}^{*}=\frac{-1}{\pi}\,\mathrm{Re}\left\{\sum_{J=1}^{4}A_{LJ}^{(1)}\left[\ln(z_J^{(1)}-s_J^{(1)})H_{JK}^{(1)}+\sum_{I=1}^{4}W_{JI}^{11}\ln(z_J^{(1)}-\bar{s}_I^{(1)})\bar{H}_{IK}^{(1)}\right]\right\}, \tag{A.21}$$

$$T_{KL}^{*}=\frac{1}{\pi}\,\mathrm{Re}\left\{\sum_{J=1}^{4}B_{LJ}^{(1)}\left[\frac{\mu_J^{(1)}n_x-n_y}{z_J^{(1)}-s_J^{(1)}}H_{JK}^{(1)}+\sum_{I=1}^{4}W_{JI}^{11}\frac{\mu_J^{(1)}n_x-n_y}{z_J^{(1)}-\bar{s}_I^{(1)}}\bar{H}_{IK}^{(1)}\right]\right\}, \tag{A.22}$$

where the matrix $\mathbf{H}$ is defined in Eq. (A.12) with the piezoelectric properties of material #1, and

$$\mathbf{W}^{11}=\mathbf{B}_{(1)}^{-1}(\mathbf{Y}_{(1)}+\bar{\mathbf{Y}}_{(2)})^{-1}(\bar{\mathbf{Y}}_{(1)}-\bar{\mathbf{Y}}_{(2)})\bar{\mathbf{B}}_{(1)} \tag{A.23}$$

(II) For source point ($s$) in material #1 ($y>0$) and field point ($z$) in material #2 ($y<0$):

$$U_{KL}^{*}=\frac{-1}{\pi}\,\mathrm{Re}\left\{\sum_{J=1}^{4}A_{LJ}^{(2)}\left[\sum_{I=1}^{4}W_{JI}^{12}\ln(z_J^{(2)}-s_I^{(1)})H_{IK}^{(1)}\right]\right\}, \tag{A.24}$$

$$T_{KL}^{*}=\frac{1}{\pi}\,\mathrm{Re}\left\{\sum_{J=1}^{4}B_{LJ}^{(2)}\left[\sum_{I=1}^{4}W_{JI}^{12}\frac{\mu_J^{(2)}n_x-n_y}{z_J^{(2)}-s_I^{(1)}}H_{IK}^{(1)}\right]\right\}, \tag{A.25}$$

with

$$\mathbf{W}^{12}=\mathbf{B}_{(2)}^{-1}(\mathbf{Y}_{(2)}+\bar{\mathbf{Y}}_{(1)})^{-1}(\bar{\mathbf{Y}}_{(1)}+\mathbf{Y}_{(1)})\mathbf{B}_{(1)} \tag{A.26}$$

(III) For source ($s$) and field ($z$) points in material #2 ($y<0$):

$$U_{KL}^{*}=\frac{-1}{\pi}\,\mathrm{Re}\left\{\sum_{J=1}^{4}A_{LJ}^{(2)}\left[\ln(z_J^{(2)}-s_J^{(2)})H_{JK}^{(2)}+\sum_{I=1}^{4}W_{JI}^{22}\ln(z_J^{(2)}-\bar{s}_I^{(2)})\bar{H}_{IK}^{(2)}\right]\right\}, \tag{A.27}$$

$$T_{KL}^{*}=\frac{1}{\pi}\,\mathrm{Re}\left\{\sum_{J=1}^{4}B_{LJ}^{(2)}\left[\frac{\mu_J^{(2)}n_x-n_y}{z_J^{(2)}-s_J^{(2)}}H_{JK}^{(2)}+\sum_{I=1}^{4}W_{JI}^{22}\frac{\mu_J^{(2)}n_x-n_y}{z_J^{(2)}-\bar{s}_I^{(2)}}\bar{H}_{IK}^{(2)}\right]\right\}, \tag{A.28}$$

where the matrix $\mathbf{H}$ is defined in Eq. (A.12) with the piezoelectric properties of material #2, and

$$\mathbf{W}^{22}=\mathbf{B}_{(2)}^{-1}(\mathbf{Y}_{(2)}+\bar{\mathbf{Y}}_{(1)})^{-1}(\bar{\mathbf{Y}}_{(2)}-\bar{\mathbf{Y}}_{(1)})\bar{\mathbf{B}}_{(2)} \tag{A.29}$$

(IV) For source point ($s$) in material #2 ($y < 0$) and field point ($z$) in material #1 ($y > 0$)

$$U^*_{KL} = \frac{-1}{\pi}\,\mathrm{Re}\left\{\sum_{J=1}^{4} A^{(1)}_{LJ}\left[\sum_{I=1}^{4} W^{21}_{JI}\,\ln(z^{(1)}_J - s^{(2)}_I)H^{(2)}_{IK}\right]\right\}, \tag{A.30}$$

$$T^*_{KL} = \frac{1}{\pi}\,\mathrm{Re}\left\{\sum_{J=1}^{4} B^{(1)}_{LJ}\left[\sum_{I=1}^{4} W^{21}_{JI}\,\frac{\mu^{(1)}_J n_x - n_y}{z^{(1)}_J - s^{(2)}_I}H^{(2)}_{IK}\right]\right\}, \tag{A.31}$$

with

$$\mathbf{W}^{21} = \mathbf{B}^{-1}_{(1)}(\mathbf{Y}_{(1)} + \bar{\mathbf{Y}}_{(2)})^{-1}(\bar{\mathbf{Y}}_{(2)} + \mathbf{Y}_{(2)})\mathbf{B}_{(2)}. \tag{A.32}$$

## References


[1] Newnham RE, Ruschau GR. Electromechanical properties of smart materials. J Intell Mat Sys Struct 1993;4:289–294.

[2] Dunn ML, Taya M. An analysis of piezoelectric composite materials containing ellipsoidal inhomogeneities. Proc R Soc Lond A 1993;443:265–287.

[3] Pak YE. Crack extension force in a piezoelectric material. J Appl Mech 1990;57:647–653.

[4] Pak YE. Force on a piezoelectric screw dislocation. J Appl Mech 1990;57:863–869.

[5] Suo Z, Kuo CM, Barnett DM, Willis JR. Fracture mechanics for piezoelectric ceramics. J Mech Phys Solids 1992;40:739–765.

[6] Dunn ML. The effects of crack face boundary conditions on the fracture mechanics of piezoelectric solids. Eng Fract Mech 1994;48:25–39.

[7] Yang W, Suo Z. Cracking in ceramic actuators caused by electrostriction. J Mech Phys Solids 1994;42:649–663.

[8] Dascalu C, Maugin GA. On the dynamic fracture of piezoelectric materials. Q J Mech Appl Math 1995;48:237–255.

[9] Hao TH, Gong X, Suo Z. Fracture mechanics for the design of ceramic multilayer actuators. J Mech Phys Solids 1996;44:23–48.

[10] Chen CQ, Shen YP, Wang XM. Exact solution of orthotropic cylindrical shell with piezoelectric layers under cylindrical bending. Int J Solids Structures 1996;33:4481–4494.

[11] Batra RC, Liang XQ, Yang JS. The vibration of a simply supported rectangular elastic plate due to piezoelectric actuators. Int J Solids Structures 1996;33:1597–1618.

[12] Lee JS, Jiang LZ. Exact electroelastic analysis of piezoelectric laminae via state space approach. Int J Solids Structures 1996;33:977–990.

[13] Bisegna P, Maceri F. An exact three-dimensional solution for simply supported rectangular piezoelectric plates. J Appl Mech 1996;63:628–638.

[14] Heyliger P, Brooks S. Exact solutions for laminated piezoelectric plates in cylindrical bending. J Appl Mech 1996;63:903–910.

[15] Dumir PC, Dube GP, Kapuria S. Exact piezoelastic solution of simply-supported orthotropic circular cylindrical panel in cylindrical bending. Int J Solids Structures 1997;34:685–702.

[16] Ha SK, Keilers C, Chang FK. Finite element analysis of composite structures containing distributed piezoceramic sensors and actuators. AIAA Journal 1992;30:772–780.

[17] Lee JS. Boundary element method for electroelastic interaction in piezoceramics. Eng Anal Bound Elements 1995;15:321–328.

[18] Lee JS, Jiang LZ. A boundary integral formulation and 2D fundamental solution for piezoelastic media. Mech Res Commun 1994;21:47–54.

[19] Chen T, Lin FZ. Boundary integral formulations for three-dimensional anisotropic piezoelectric solids. Computat Mech 1995;15:485–496.

[20] Tiersten HF. Linear piezoelectric plate vibrations. New York: Plenum, 1969.

[21] Barnett DM, Lothe J. Dislocations and line charges in anisotropic piezoelectric insulators. Phys Stat Sol B 1975;67:105–111.

[22] Pan E, Amadei B. A 3-D boundary element formulation of anisotropic elasticity with gravity. Appl Mat Model 1996;20:114–120.

[23] Aliabadi MH. Boundary element formulations in fracture mechanics. Appl Mech Rev 1997;50:83–96.

[24] Pan E, Amadei B. Fracture mechanics analysis of cracked 2-D anisotropic media with a new formulation of the boundary element method. Int J Fracture 1996;77:161–174.

[25] Portela A, Aliabadi MH, Rooke DP. The dual boundary element method: Effective implementation for crack problems. Int J Numer Meth Eng 1992;33:1269–1287.

[26] Pan E. A general boundary element analysis of 2-D linear elastic fracture mechanics. Int J Fracture, in press.

[27] Tsamasphyros G, Dimou G. Gauss quadrature rules for finite part integrals. Int J Numer Meth Eng 1990;30:13–26.

[28] Sosa HA, Castro MA. On concentrated loads at the boundary of a piezoelectric half plane. J Mech Phys Solids 1994;42:1105–1122.

[29] Chung MY, Ting TCT. Line force, charge, and dislocation in anisotropic piezoelectric composite wedges and spaces. J Appl Mech 1995;62:423–428.

[30] Sollero P, Aliabadi MH, Rooke DP. Anisotropic analysis of cracks emanating from circular holes in composite laminates using the boundary element method. Eng Fracture Mech 1994;49:213–224.

[31] Suo Z. Singularities, interfaces and cracks in dissimilar anisotropic media. Proc R Soc Lond A 1990;427:331–358.

[32] Eshelby JD, Read WT, Shockley W. Anisotropic elasticity with applications to dislocations theory. Acta Metal 1953;1:251–259.